First-principles study of strain effect on the formation and electronic structures of oxygen vacancy in $SrFeO_2$*

Wei Zhang(张玮)[1,†] and Jie Huang(黄洁)[2]

[1] *Physics Group of Department of Criminal Science and Technology, Nanjing Forest Police College, Nanjing* 210023, *China*
[2] *Department of Physics, Nanjing Normal University, Nanjing* 210023, *China*

(Received 4 December 2015; revised manuscript received 12 January 2016; published online 5 April 2016)

Motivated by recent experimental observations of metallic conduction in the quasi-two-dimensional $SrFeO_2$, we study the epitaxial strain effect on the formation and electronic structures of oxygen vacancy (V_o) by first-principles calculations. The bulk $SrFeO_2$ is found to have the G-type antiferromagnetic ordering (G-AFM) at zero strain, which agrees with the experiment. Under compressive strain the bulk $SrFeO_2$ keeps the G-AFM and has the trend of Mott insulator-metal transition. Different from most of the previous similar work about the strain effect on V_o, both the tensile strain and the compressive strain enhance the V_o formation. It is found that the competitions between the band energies and the electrostatic interactions are the dominant mechanisms in determining the V_o formation. We confirm that the V_o in $SrFeO_2$ would induce the n-type conductivity where the donor levels are occupied by the delocalized $d_{x^2-y^2}$ electrons. It is suggested that the vanishing of n-type conductivity observed by the Hall measurement on the strained films are caused by the shift of donor levels into the conduction band. These results would provide insightful information for the realization of metallic conduction in $SrFeO_2$.

Keywords: first-principles calculations, strain, oxygen vacancy, electronic structure

PACS: 71.15.Mb, 61.72.jd, 71.55.–i, 75.50.Ee **DOI:** 10.1088/1674-1056/25/5/057103

1. Introduction

Transition-metal oxides (TMOs) have been widely studied because of the peculiar physics and the novel functions found in these materials. Among these TMOs, the Fe related oxides are one of the most extensively studied systems. Here, we focus on the newly synthesized compound $SrFeO_2$, which is the first ternary earth alkaline oxoferrate.[1,2] Unlike the conventional ABO_3 perovskite structure, the lack of apical oxygen made $SrFeO_2$ have the infinite-layer structure with a square-planar coordination (Fig. 1). This layered structure was isotypic with $SrCuO_2$, the parent compound for the high temperature (high-T_c) superconductor. In spite of this quasi-two-dimensional structure, $SrFeO_2$ showed the three-dimensional G-type antiferromagnetic ordering (G-AFM) with a very high Neel temperature ($T_N = 473$ K). According to the crystal field theory,[3] the down-spin electron of high-spin $Fe^{2+}(d^6)$ was expected to occupy the degenerate (d_{xz}, d_{yz}) orbitals, and $SrFeO_2$ should be subject to Jahn–Teller distortion when the temperature was lowered. However, in experiment, $SrFeO_2$ was found to maintain the $P4/mmm$ symmetry down to 4.2 K,[1] which showed a nostructural instability. Besides, the T_N often decreased sharply when the dimensionality decreased. Such high T_N in a two-dimensional system was unexpected, which attracted the attention of researchers. Xiang *et al.*[4] regarded that the d_z^2 orbital was the lowest energy orbital and the last down-spin electron occupied the d_z^2 orbital. Pruneda *et al.*[5] also found the double occupation of the d_z^2 orbital of Fe^{2+}, but they attributed the $(d_z^2)^2$ occupations to the reduction of spin splitting of d_z^2 orbitals. Kawakami *et al.*[6] reported the high pressure induced spin transition in $SrFeO_2$, where the high-spin Fe^{2+} ($S = 2$) changed to the intermediate-spin state ($S = 1$) at ∼33 GPa. This spin transition was simultaneously accompanied by an AFM–FM transition and a Mott insulator–metal transition. Ju *et al.*[7] found that $SrFeO_2$ showed giant optical anisotropy. It was found[8] that the substitution of Fe by Co or Mn can keep the tetragonal structure unchanged up to the solubility limit of $x = 0.3$. The neutron diffraction[9] at 5 K revealed that the long-range magnetic order disappeared in $SrFe_{0.5}Ru_{0.5}O_2$. Horigane *et al.*[10] found the suppression of magnetic coupling by in-plane buckling. It was also reported that the FeO_2-terminated (001) surface underwent a magnetic reconstruction consisting of a spin-flip process.[11] Despite extensive research on this layered TMO, previous work mostly focused on the bulk $SrFeO_2$, and very little was known about the defect $SrFeO_2$. So far there has been no study of the oxygen vacancy (V_o) in $SrFeO_2$. V_o is one of the fundamental and intrinsic defects in TMOs, and it often has a crucial impact on the properties of TMOs. For example, the V_o can enable ionic conductivity in the solid oxide fuel cell (SOFC) cathodes, oxygen sensors, and mixed conducting membranes.[12,13] Therefore, the lack of knowledge of V_o in $SrFeO_2$ would inhibit the technological applications and fundamental understanding of this quasi-two-dimensional material.

*Project supported by the Creative Plan Project of Nanjing Forest Police College, China (Grant Nos. 201512213045xy and 201512213007x).
†Corresponding author. E-mail: zhangw@nfpc.edu.cn
© 2016 Chinese Physical Society and IOP Publishing Ltd

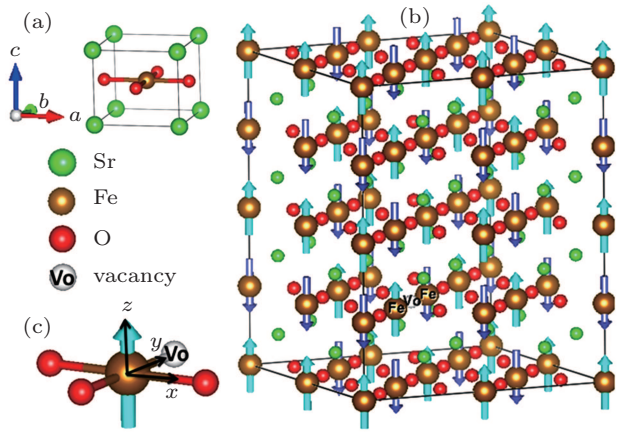


Fig. 1. (color online) (a) The four-atom primitive cell of tetragonal $SrFeO_2$. (b) The $2\sqrt{2}\times 2\sqrt{2}\times 4$ supercell of $SrFeO_2$ with G-AFM. The arrows denote the up-spin and down-spin. (c) Local coordinate of Fe–O bonds.

On the other hand, the functional behavior of TMOs can be improved when they are prepared as thin films. The enhanced behavior is usually attributed to the strain introduced by the substrate with different lattice constants. The epitaxial strain would affect the bond lengths and/or the bond angles, which finally changes the electronic structures, the magnetic properties and so on. Importantly, as $SrFeO_2$ was isotypic with $SrCuO_2$ where the high-T_c could be induced by carrier doping,[14] the researchers concentrated on the realization of metallic conduction in$SrFeO_2$ by chemical substitution.[15–18] However, the obtained compounds were still insulators. Recently, the single-crystalline epitaxial $SrFeO_2$ thin films were grown on the perovskite substrates with various lattice constants.[19] Metallic conduction was found on the lattice-matched $KTaO_3$ (001) substrate, and Hall measurements showed that the conduction carriers are n-type. Katayama *et al.* confirmed that the metallic conduction was an intrinsic property of $SrFeO_2$ film and speculated the carriers were supplied by V_o as there were V_o's in their films. However, they did not observe n-type conductivity on the lattice-mismatched substrates. Thus, it is worth examining whether the V_o of $SrFeO_2$ can induce the n-type conductivity and how the behavior of V_o is affected by the epitaxial strain. In this work, we provide a first-principles survey of the following questions. (i) Do the bulk $SrFeO_2$ have a magnetic transition under strain? (ii) How difficult is it to form a V_o in $SrFeO_2$? (iii) Does V_o act as electron donors to mobile conducting states at the Fermi level in $SrFeO_2$? (iv) If the V_o in $SrFeO_2$ induces the n-type conductivity, how does the strain affect the performance of the n-type conductivity?

The remainder of this paper is organized as follows. In Section 2 we describe the calculation method used throughout this work. In Section 3 we first study the properties of bulk $SrFeO_2$ under strain, then discuss the strain induced changes of formation energy of V_o. After that we present our results for the electronic structures of V_o under strain. Finally, the conclusion is given in Section 4.

2. Computational method

First-principles calculations are performed using the projector augmented wave (PAW) method,[20] as implemented in the Vienna *ab initio* simulation package (VASP).[21,22] The exchange–correlation functional is treated by the generalized gradient approximation (GGA).[23] The Hubbard U correction[24] is applied to Fe 3d electrons. We use $U_{\rm eff}$ = 4 eV[5] to reproduce the experimentally determined electronic and magnetic properties of bulk $SrFeO_2$. The valence electron configurations are Sr ($4s^24p^65s^2$), Fe ($3p^63d^63s^2$), and O ($2s^22p^4$). To model the V_o, we construct a $2\sqrt{2}\times 2\sqrt{2}\times 4$ (~ 11.4 Å$\times 11.4$ Å$\times 14$ Å) supercell with 128 atoms. A plane-wave cutoff of 600 eV is used throughout. A 2×2×2 and a 4×4×4 k-mesh[25] are used for the structural relaxations and density of states (DOS) calculations, respectively. The crystal structures are relaxed until the inter-atomic forces are smaller than 0.01 eV/Å and the convergence criteria for energy is 10^{-5} eV. To simulate the epitaxial strain in a thin film constrained on a cubic (001)-oriented substrate, we vary the in-plane lattice constants ($a = b$) of the tetragonal cell, and relax the out-of-plane lattice constant c and all internal coordinates. The strained structures are relaxed until the stresses along the out-of-plane direction are less than 0.1 kbar. The strain is defined as $\varepsilon = a/a_0 - 1$, where a_0 corresponds to the optimized lattice constant without strain.

The formation energy ($E_{\rm form}$) of V_o is calculated according to the following formula: $E_{\rm form}(\varepsilon,\ V_o) = E_{\rm tot,Vo} - E_{\rm tot,bulk} + \mu_O$, where μ_O is the chemical potential of oxygen. The $E_{\rm tot,bulk}$ and $E_{\rm tot,Vo}$ denote the total energy of the bulk simulation cell and that containing V_o, respectively.

3. Results

3.1. Bulk $SrFeO_2$

We first reproduce the experimentally determined properties of bulk $SrFeO_2$. As shown in Tables 1 and 2, the calculated lattice constants, band gap, and magnetic moment overall agree with the experiment and previous theoretical work.[5] Then we study the strain effect on the bulk $SrFeO_2$. The $SrFeO_2$ thin film may be grown on various substrates. Except for the lattice-matched $KTaO_3$ substrate,[1,2,19] the practical substrate lattice constants are smaller than 3.99 Å, such as 3.91 Å ($SrTiO_3$),[19,28] 3.79 Å ($LaAlO_3$),[29] 3.94 Å ($DyScO_3$),[19,30] etc. Therefore, the compressive strains are introduced up to −0.06. The tensile strains are also introduced for comparison. To determine the magnetic orderings under strain, we consider the A-AFM, C-AFM, G-AFM, and FM. As shown in Fig. 2, for the G-AFM, both the intralayer nearest neighbor (NN) interactions and the interlayer NN interactions are AFM. For the A-AFM, the intralayer NN interactions are FM, while the interlayer NN interactions are AFM. For the C-AFM, the intralayer NN interactions are AFM while the

interlayer NN interactions are FM. From Tables 1 and 2 we can see that the G-AFM has the lowest total energy, indicating that the G-AFM is the magnetic ground state in the strain range we studied. Table 1 also shows the bulk $SrFeO_2$ has the G-AFM at zero strain, which agrees with the experiment.[1] From Fig. 3 we can see both the magnetic moment and the volume decrease with increasing strain. The change of volume indicates that $SrFeO_2$ does not have a perfect Poisson ratio, as a material with an ideal Poisson ratio has a constant volume with strain. This is also reflected in the lattice constants. Due to the high symmetric positions of Fe and O, the Fe–O bonds synchronously expand (reduce) with increasing (decreasing) strain, while the O–Fe–O bond angles keep constant (90°) on the strain range. Consistent with previous work,[4,5] the density of states (DOS) in Fig. 4(b) shows that the bulk $SrFeO_2$ displays a Mott–Hubbard band gap, where the down Fe $3d_z^2$ states locate right below the gap and other down 3d orbitals locate above it. The electronic configurations (see Fig. 4(b-2)) are $(d_{xy})^1(d_{yz}d_{xz})^2(d_{x^2-y^2})^1(d_{z^2})^1$ for the up-spin $Fe^{2+}(d^6)$ ion while the sixth down-spin electron occupies the d_z^2 orbital. As shown in Figs. 4(a) and 4(c), when the tensile strain is imposed on $SrFeO_2$, the degenerate $d_{yz}d_{xz}$ states in the conduction band (CB) are pushed into the higher energy levels, thus the insulator character is enhanced with increasing tensile strain.

Table 1. The calculated properties of bulk $SrFeO_2$ without strain. For comparison, the experimental values and previous theoretical values are also provided. The units of $a(b)$ and c are Å. The units of M_{Fe} and E_{gap} are μB and eV, respectively.

Property	$a(b)$	c	M_{Fe}	E_{gap}
Present work	4.04	3.49	3.65	1.1
Experiment[1,27]	3.99	3.47	3.6	1.3
Theory[5]	4.01	3.42	3.6	1.1

Table 2. The calculated total energies (meV/f.u.) of bulk $SrFeO_2$ at different strains. E_G, E_A, E_C, and E_F denote the total energies of G-AFM, A-AFM, C-AFM, and FM, respectively.

Strain	E_G	E_A	E_C	E_F
–0.06	0	116.86	20.13	115.88
–0.04	0	129.92	23.7	132.54
–0.02	0	124.32	20.19	128.13
0	0	106.66	19.7	113.97
0.02	0	91.33	19.1	99.67
0.04	0	76.78	18.53	84.01
0.06	0	61.84	17.88	71.28

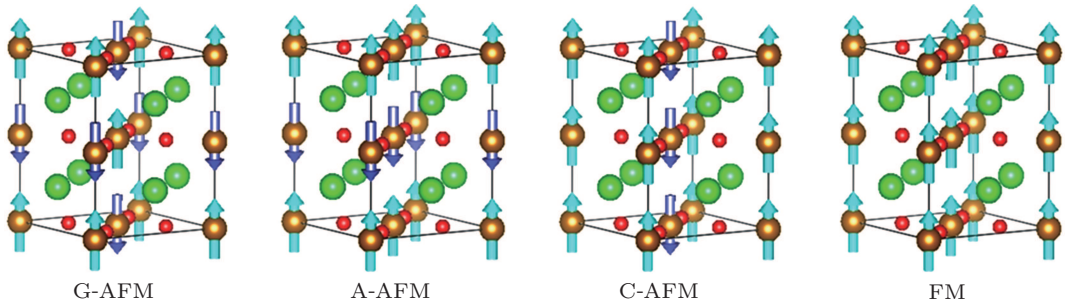


Fig. 2. (color online) Schematic view of different magnetic orderings. For clarity the $\sqrt{2}\times\sqrt{2}\times 2$ supercell of $SrFeO_2$ is used.

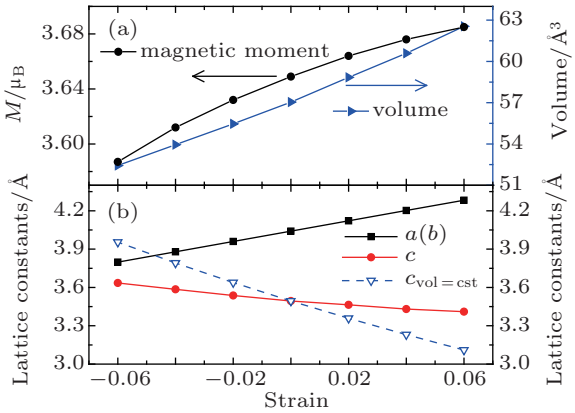


Fig. 3. (color online) Evolution of structural and magnetic properties with strain in bulk $SrFeO_2$. (a) The relaxed volume (vol) and magnetic moment. (b) Lattice constants. The dashed line shows the c-axis lattice constant (cst) for a material with an ideal Poisson ratio.

On the contrary, the compressive strain makes the $d_{yz}d_{xz}$ states in the CB come nearer with respect to the valence band maximum (VBM), thus the band gap decreases with increasing compressive strain. At the same time, the separation between the $d_{x^2-y^2}$ states and the down d_{z^2} states becomes larger around the Fermi level. When the compressive strain increases up to −0.06, the band gap nearly comes to zero (not shown), the $d_{x^2-y^2}$ states also come nearer with respect to the Fermi level. A Mott-type insulator–metal transition (IMT), where the $d_{x^2-y^2}$ orbital would cross the Fermi level, is expected if we continue to increase the compressive strain, which is similar to the case of IMT at hydrostatic pressure.[6,31] Note that tests are performed at −0.08 and −0.1 strain, and we find the occupations of $d_{x^2-y^2}$ states at the Fermi level, but the large strain values which may not be very practical are beyond the scope of the present work. Figure 5 shows the evolution of exchange interactions obtained using the classic Heisenberg spin model: $H = -J_1\sum S_iS_j - J_2\sum S_iS_j - J_3\sum S_iS_j$, $S_{i(j)} = \pm 2$.

We consider the intralayer NN exchange interactions J_1, the interlayer NN exchange interactions J_2, and the interlayer next nearest neighbor (NNN) exchange interactions J_3. The calculated values at zero strain agree well with previous work.[5] The exchange interactions show the anisotropic behavior where J_1 is about three times larger than J_2,

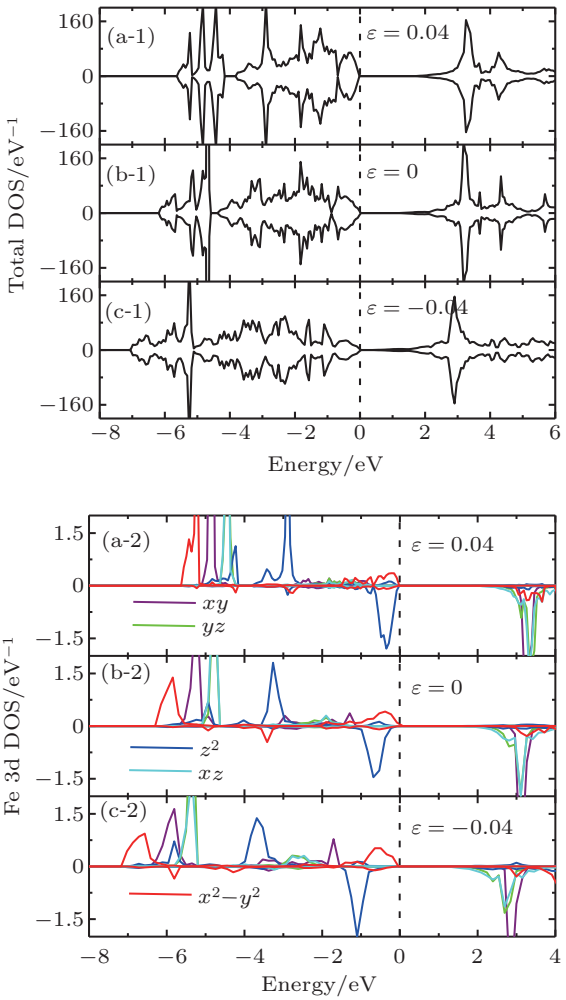


Fig. 4. (color online) (a-1), (b-1), (c-1), and (d-1) Total DOS and (a-2), (b-2), (c-2), and (d-2) orbital-resolved DOS of bulk $SrFeO_2$.

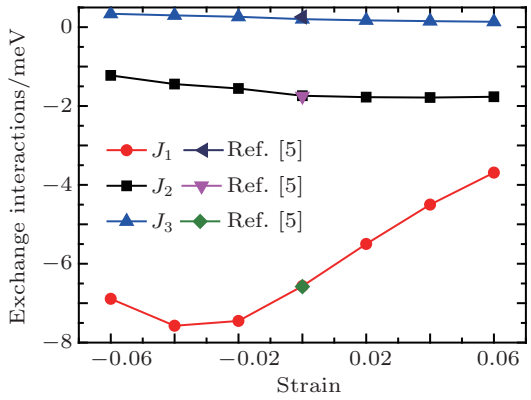


Fig. 5. (color online) Exchange interactions with respect to the strain. The data (zero strain) of Ref. [5] are provided for comparison.

indicating the dominant role of intralayer superexchange interactions. It is interesting to note that the strength (absolute value) of J_1 shows a decrease trend at -0.06 strain. This may imply the instability of G-AFM at very large strain as the AFM–FM transition has been found at high pressure.[6,31]

3.2. Defect $SrFeO_2$: Formation energy of V_o

In the tetragonal $SrFeO_2$ structure (see Fig. 1), the oxygen positions are equivalent to each other. Therefore, an arbitrary O atom is removed from the supercell to calculate the E_{form} of V_o. In extreme oxidation conditions (oxygen rich), the μ_O is subject to an upper bound given by the energy of O in an O_2 molecule, i.e., $\mu_O = (1/2)E_{O_2}$. In extreme reduction conditions (oxygen deficient), μ_{Sr} and μ_{Fe} are subject to an upper bound given by the energy of Sr and Fe in the bulk phases ($\mu_{Sr} = E_{Sr,bulk}$, $\mu_{Fe} = E_{Fe,bulk}$). Thus in this condition, $\mu_O = [E_{tot,bulk(f.u.)} - \mu_{Sr} - \mu_{Fe}]/2$. The calculated V_o formation energy is shown in Fig. 6. We can see the E_{form} is relatively high. Thus, the V_o concentration is expected to be low in equilibrium condition. Although the E_{form} is positive (e.g., 5.1 eV, zero strain, oxygen rich), it is comparable with the E_{form} (zero strain, oxygen rich) of some typical TMOs, such as HfO_2[32] (5.93 eV), ZnO[33] (5.37 eV), ZrO_2[34] (5.97 eV), etc. The V_o is often unintentionally introduced during the growth or annealing process of these TMOs.[35,36] Thus, the V_o of $SrFeO_2$ should be stably formed under certain growth conditions.

Generally speaking, the increase in bond lengths and volumes associated with the tensile strain is likely to decrease the formation energies of V_o due to the decreased Coulomb interactions between ions.[37] It is also believed that the remaining electrons caused by V_o would strengthen the pressure of the electron gas and thus induce an intrinsic compressive stress in the unrelaxed lattice.[38] Therefore, the formation energy is expected to increase in the compressive strain range, and the tensile strain would relieve the intrinsic compressive stress and promote to create the V_o, which has been widely reported in previous similar work.[39,40] As expected, the V_o formation energy decreases with increasing tensile strain, as shown in Fig. 6. However, we can see from Fig. 6 that the compressive strain also decreases the formation energy. Especially in the compressive strain range the formation energy shows a sharper decrease than that of the tensile strain range. To understand this phenomenon, we first examine the structural relaxations around V_o at each strain. As shown in Table 3 and Fig. 7(a), the removal of oxygen would unscreen the positive Fe ions around V_o by the Coulomb interactions,

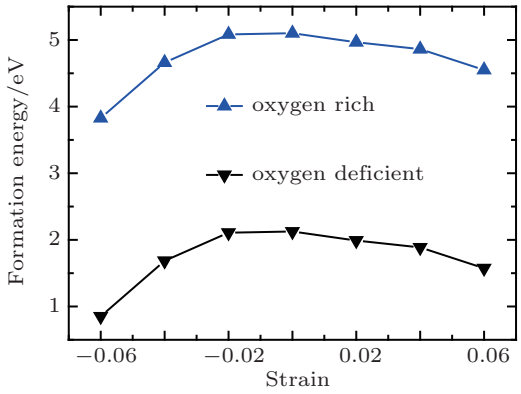


Fig. 6. (color online) Formation energy of V_o as a function of strain.

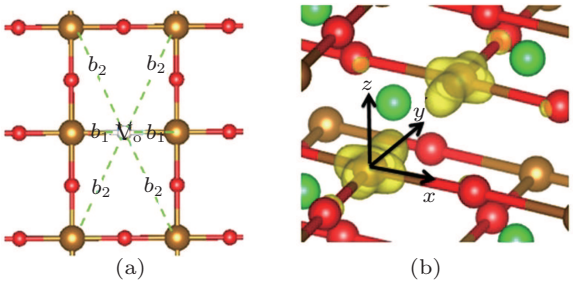


Fig. 7. (color online) (a) Local structure around V_o. b_1 and b_2 are the bond lengths (Å). (b) Partial charge density of the defect levels shown in Fig. 9(b-2). The isosurface value is 0.015 e^-/Bohr^3.

Table 3. Structural relaxations around V_o. Δ denotes the changes of $b_1(b_2)$ before and after relaxations. The units of b_1 (b_2) are Å.

Strain	b_1		Δb_1	b_2		Δb_2
	before	after		before	after	
–0.06	1.9	1.91	0.01	4.25	4.24	–0.01
–0.04	1.94	2.03	0.09	4.34	4.32	–0.02
–0.02	1.98	2.13	0.15	4.43	4.42	–0.01
0	2.02	2.05	0.03	4.52	4.51	–0.01
0.02	2.06	2.19	0.13	4.61	4.60	–0.01
0.04	2.1	2.29	0.19	4.7	4.69	–0.01
0.06	2.14	2.22	0.08	4.79	4.76	–0.03

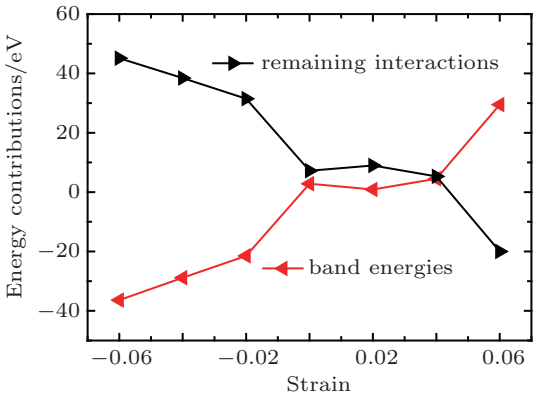


Fig. 8. (color online) Decomposition of E_{form} into its contributions.

which results in significant outward relaxations for the two NN Fe ions. For the four NNN Fe ions, the distances between them ($\sim$ 9 Å) are far larger than that of the two NN Fe ions, and the non-screen effect is smaller, thus the four NNN Fe ions show a slight inward relaxation. Although the relaxation patterns are similar for the compressive strain and the tensile strain, we note the outward relaxations are larger in the tensile strain range when the tensile strain is larger than 0.02, which may indicate the dominant role of the rapidly decreased Coulomb interactions in the tensile strain range. Noting that the decreased bond lengths and volumes caused by compressive strain would make the electronic structures more complex due to the enhanced overlap between orbitals, and thus change the electronic energies which may compensate the increased Coulomb interactions. To confirm this assumption, we decompose the V_o formation energy into its components in Fig. 8. We can see that in the compressive strain range the rapidly decreased band energies can overcompensate the increased remaining energies (mainly electrostatic), which induces the decrease of formation energy. On the contrary, in the tensile strain range the rapidly decreased remaining energies overcompensate the increased band energies when the tensile strain is larger than 0.02, indicating the dominant role of the electrostatic interactions in the tensile strain range. Therefore, the competitions between the band energies and the electrostatic interactions are the dominant mechanisms in determining the V_o formation.

3.3. Defect $SrFeO_2$: electronic structures of V_o

As shown in Fig. 9, the V_o formation produces a large shift of the Fermi level. According to the crystal field theory, the removal of oxygen will make the Fe 3d orbitals with the y component fall in energy level. The $d_{x^2-y^2}$ orbitals fall the most, as the electrons of $d_{x^2-y^2}$ orbitals are concentrated in lobes along the directions of Fe–O bonds. Thus, the remaining electrons of V_o mainly occupy the empty down-spin $d_{x^2-y^2}$ orbitals (see Figs. 7(b) and 9(b-2)) and the resulting donor levels locate right below the CBM, indicating the character of n-type conductivity. Comparing with the DOS (see Fig. 4(b-2)) of bulk $SrFeO_2$, the $d_{x^2-y^2}$ electrons become delocalized, as can be seen from the wide distribution of more peaks in the energy range. Therefore, the mobility of the conduction electrons is expected to be large. With the increase of compressive strain, the intralayer superexchange interactions between $d_{x^2-y^2}$ states through O p_σ increase, which lifts the energy levels of the $d_{x^2-y^2}$ orbitals. Thus, the occupations of the conduction electrons rapidly decrease when the compressive strain is imposed (Fig. 9(c)). When the compressive strain increases to -0.06, the Fermi level is occupied mainly by the Sr d electrons while the down-spin $d_{x^2-y^2}$ states are fully pushed into the CB. The tensile strain (Fig. 9(a)) displays the behavior which favors the occupations of $d_{x^2-y^2}$ orbitals for the conduction electrons. This is because the decreased intralayer superexchange interactions further decrease the energy level of $d_{x^2-y^2}$ orbitals. Even so, the separation between the donor level and the CBM becomes larger and the donor level approximately shifts to the middle of the enlarged gap at 0.06 strain. Thus, the n-type conductivity becomes poor under tensile strain. Finally, based on the above discussion, we propose a possible explanation for the observations of the Hall experiment. As reported in Fig. 6, the V_o concentration is expected to be low in $SrFeO_2$. In Ref. [19], Katayama *et al.* found the n-type conductivity on the lattice-matched $KTaO_3$ substrate which corresponds to the case of zero strain. The $DyScO_3$ substrate (3.94 Å) and the $SrTiO_3$ substrate (3.91 Å) would introduce -0.01 and -0.04 compressive strain. As discussed in Fig. 9, the delocalized $d_{x^2-y^2}$ electrons are rapidly pushed into the CB once the compressive strain is applied. Although the DOS at -0.06 strain

displays the metallic character, the Fermi level is mainly occupied by the localized Sr d electrons. Therefore, no n-type conductivity is found in the strained films.

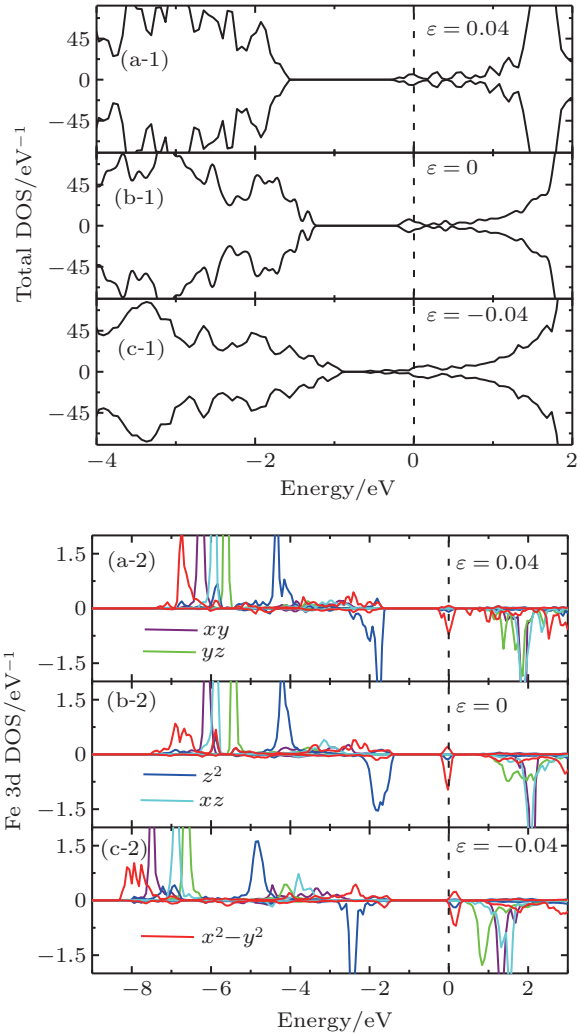


Fig. 9. (color online) (a-1), (b-1), (c-1), and (d-1) Total DOS and (a-2), (b-2), (c-2), and (d-2) orbital-resolved DOS of defect $SrFeO_2$ with V_o.

4. Conclusion and perspectives

In summary, we study the epitaxial strain effect on the formation and electronic structures of V_o in $SrFeO_2$ by first-principles calculations. It is found that the bulk $SrFeO_2$ has the G-AFM at zero strain, which agrees with the experiment. Under compressive strain the bulk $SrFeO_2$ keeps the G-AFM and has the trend of Mott insulator–metal transition. We find both the tensile strain and the compressive strain enhance the V_o formation which is different from most of the previous similar work about the strain effect on V_o. The competition between the band energies and the electrostatic interactions is found to be the dominant mechanism in determining the formation of V_o. The V_o in $SrFeO_2$ is confirmed to induce the n-type conductivity where the donor levels are occupied by the delocalized $d_{x^2-y^2}$ electrons. Our results suggest that the vanishing of n-type conductivity observed by the Hall measurement on the strained films is caused by the shift of donor levels into the conduction band. The calculations would provide insightful information for the realization of metallic conduction in $SrFeO_2$.

Acknowledgment

We acknowledge the supercomputer time provided by the HPC Center of Department of Physics of Nanjing Normal University.

References

[1] Tsujimoto Y, Tassel C, Hayashi N, Watanabe T, Kageyama H, Yoshimura K, Takano M, Ceretti M, Ritter C and Paulus W 2007 *Nature* **450** 1062
[2] Inoue S, Kawai M, Shimakawa Y, Mizumaki M, Kawamura N, Watanabe T, Tsujimoto Y, Kageyama H and Yoshimura K 2008 *Appl. Phys. Lett.* **92** 161911
[3] Wells A F 1975 *Structural Inorganic Chemistry* (Oxford: Oxford University Press)
[4] Xiang H J, Wei S H and Whangbo M H 2008 *Phys. Rev. Lett.* **100** 167207
[5] Pruneda J M, Íñiguez J, Canadell E, Kageyama H and Takano M 2008 *Phys. Rev. B* **78** 115101
[6] Kawakami T, Tsujimoto Y, Kageyama H, Chen X Q, Fu C L, Tassel C, Kitada A, Suto S, Hirama K, Sekiya Y, Makino Y, Okada T, Yagi T, Hayashi N, Yoshimura K, Nasu S, Podloucky R and Takano M 2009 *Nat. Chem.* **1** 371
[7] Ju S and Cai T Y 2009 *Appl. Phys. Lett.* **94** 061902
[8] Seinberg L, Yamamoto T, Tassel C, Kobayashi Y, Hayashi N, Kitada A, Sumida Y, Watanabe T, Nishi M, Ohoyama K, Yoshimura K, Takano M, Paulus W and Kageyama H 2011 *Inorg. Chem.* **50** 3988
[9] Romero F D, Burr S J, McGrady J E, Gianolio D, Cibin G and Hayward M A 2013 *J. Am. Chem. Soc.* **135** 1838
[10] Horigane K, Llobet A and Louca D 2014 *Phys. Rev. Lett.* **112** 097001
[11] Lu H S, Cai T Y, Ju S and Gong C D 2015 *J. Phys. Chem. C* **119** 17673
[12] Bouwmeester H J M 2003 *Catal. Today* **82** 141
[13] Fleig J 2003 *Annu. Rev. Mater. Res.* **33** 361
[14] Smith M G, Manthiram A, Zhou J, Goodenough J B and Markert J T 1991 *Nature* **351** 549
[15] Tamura R, Kawashima N, Yamamoto T, Tassel C and Kageyama H 2011 *Phys. Rev. B* **84** 214408
[16] Yamamoto T, Kobayashi Y, Hayashi N, Tassel C, Saito T, Yamanaka S, Takano M, Ohoyama K, Shimakawa Y, Yoshimura K and Kageyama H 2012 *J. Am. Chem. Soc.* **134** 11444
[17] Retuerto M, Jiménz-Villacorta F, Martínez-LopeM J, Fernández-Díaz M T and Alonso J A 2011 *Inorg. Chem.* **50** 10929
[18] Matsuyama T, Chikamatsu A, Hirose Y, Fukumura T and Hasegawa T 2011 *Appl. Phys. Express* **4** 013001
[19] Katayama T, Chikamatsu A, Hirose Y, Kumigashira H, Fukumura T and Hasegawa T 2014 *J. Phys. D: Appl. Phys.* **47** 135304
[20] Blöchl P E 1994 *Phys. Rev. B* **50** 17953
[21] Kresse G and Furthmüller J 1996 *Phys. Rev. B* **54** 11169
[22] Kresse G and Joubert D 1999 *Phys. Rev. B* **59** 1758
[23] Perdew J P, Burke K and Ernzerhof M 1997 *Phys. Rev. Lett.* **78** 1396
[24] Dudarev S L, Botton G A, Savrasov S Y, Humphreys C J and Sutton A P 1998 *Phys. Rev. B* **57** 1505
[25] Monkhorst H J and Pack J D 1976 *Phys. Rev. B* **13** 5188
[26] de Walle C G V and Neugebauer J 2004 *J. Appl. Phys.* **95** 3851
[27] Chikamatsu A, Matsuyama T, Hirose Y, Kumigashira H, Oshima M and Hasegawa T 2012 *J. Electron Spectrosc. Relat. Phenom.* **184** 547
[28] Béa H, Bibes M, Barthélémy A, Bouzehouane K, Jacquet E, Khodan A, Contour J P, Fusil S, Wyczisk F, Forget A, Lebeugle D, Colson D and Viret M 2005 *Appl. Phys. Lett.* **87** 072508
[29] Martin L W, Zhan Q, Suzuki Y, Ramesh R, Chi M F, Browning N, Mizoguchi T and Kreisel J 2007 *Appl. Phys. Lett.* **90** 062903
[30] Wordenweber R K R, Hollmann E and Schubert J 2007 *J. Appl. Phys.* **102** 044119
[31] Rahman M, Nie Y Z and Guo G H 2013 *Inorg. Chem.* **52** 12529
[32] Chen W, Sun Q Q, Ding S J, Zhang D W and Wang L K 2006 *Appl. Phys. Lett.* **89** 152904

[33] Lu Y B, Dai Y, Wei W, Zhu Y T and Huang B B 2013 *Chem. Phys. Chem.* **14** 3916

[34] Zhao S J, Xue J M, Wang Y G and Yan S 2012 *J. Appl. Phys.* **111** 043514

[35] Freysoldt C, Grabowski B, Hickel T, Neugebauer J, Kresse G, Janotti A and van de Walle C G 2014 *Rev. Mod. Phys.* **86** 253

[36] van de Walle C G and Janotti A 2011 *Phys. Status Solidi B* **248** 19

[37] Aschauer U, Pfenninger R, Selbach S M, Grande T and Spaldin N A 2013 *Phys. Rev. B* **88** 054111

[38] Zhu J, Liu F, Stringfellow G B and Wei S H 2010 *Phys. Rev. Lett.* **105** 195503

[39] Yang Q, Cao J X, Ma Y, Zhou Y C, Jiang L M and Zhong X L 2013 *J. Appl. Phys.* **113** 184110

[40] Ma D W, Lu Z S, Tang Y N, Li T X, Tang Z J and Yang Z X 2014 *Phys. Lett. A* **378** 2570